State Estimation for Kite Power Systems with Delayed Sensor Measurements ⋆

Max Polzin * **Tony A. Wood** *,1 **Henrik Hesse** ** **Roy S. Smith** *

* *Automatic Control Laboratory (IfA), ETH Zurich, Physikstrasse 3, 8092 Zurich, Switzerland.*
E-mail: {polzinm, woodt, rsmith}@control.ee.ethz.ch.
** *Aerospace Systems, University of Glasgow (Singapore), 510 Dover Road, Singapore 139660 (formerly at IfA, ETH Zurich).*
E-mail: henrik.hesse@glasgow.ac.uk.

Abstract: We present a novel estimation approach for airborne wind energy systems with ground-based control and energy generation. The estimator fuses measurements from an inertial measurement unit attached to a tethered wing and position measurements from a camera as well as line angle sensors in an unscented Kalman filter. We have developed a novel kinematic description for tethered wings to specifically address tether dynamics. The presented approach simultaneously estimates feedback variables for a flight controller as well as model parameters, such as a time-varying delay. We demonstrate the performance of the estimator for experimental flight data and compare it to a state-of-the-art estimator based on inertial measurements.

Keywords: Airborne wind energy, renewable energy systems, Kalman filters, robot kinematics, delay estimation, parameter estimation

1. INTRODUCTION

The idea of harvesting high-altitude winds has existed since the energy crisis in the late 1970s, Goela (1979). Yet high-altitude wind remains a vast, untapped renewable source of energy. Over the last decade, an increasing number of research groups and companies have developed working prototypes to convert the energy of winds up to 500m altitude into electricity, Cherubini et al. (2015). These so called Airborne Wind Energy (AWE) systems aim to convert the aerodynamic forces generated by an airborne structure into electrical energy.

In this work, we consider two-line AWE systems with ground-based actuation and generation, e.g. Luchsinger et al. (2016). Actuation and energy generation occurs at a ground station (GS) to which a wing is connected by tethers. The wing is actuated at the GS which contains a drum and motor for each line. The motion of the tethers over the drums at the GS is used to generate power. Steering of the wing is achieved through differential tether lengths. This system can operate with conventional soft wings, Zgraggen (2014), or more aerodynamically efficient rigid wings, Luchsinger et al. (2016).

Energy generation occurs in a two-phase power cycle. During the first phase, called **traction**, the wing is flown approximately perpendicular to the wind direction in crosswind conditions, Fagiano et al. (2014b). To avoid twisting of tethers, the wing is typically flown on a figures-of-eight trajectory. In traction, large aerodynamic forces unreel the tethers while electric power is generated. Once a maximum tether length has been reached, the wing is stabilized and rewound under low aerodynamic forces. This second phase is referred to as **retraction** phase. When a minimum line length is reached, the cycle is repeated, leading to a net power generation.

To achieve fully autonomous energy generation, automatic flight control of the wing becomes a key problem in AWE. The automatic flight controller of the AWE system described in Luchsinger et al. (2016) is based on the controllers in Fagiano et al. (2014b) and Zgraggen et al. (2015). It implements a guidance strategy based on the wing position and flight direction to fly figures-of-eight in traction phases and achieve a stable flight during retraction phases.

An estimator fuses measurements from sensors mounted on the wing and at the GS in order to compute crucial feedback variables. The difficulty of the estimation problem arises from the nonlinear dynamics, wide speed ranges, large accelerations, and fast changes of direction that the wing experiences during operation, Fagiano et al. (2014b).

A complementary filter to fuse measurements from sensors attached to the lead-outs of the tethers at the GS and of an inertial measurement unit (IMU) has been presented in Erhard and Strauch (2013b). The authors note that acceleration of the wing disrupted their estimates of the gravity vector, which is required for attitude estimation.

Many estimation schemes use position measurements from the Global Positioning System (GPS) and fuse measurements from an IMU to estimate the wing state, Gros et al. (2012). Jehle and Schmehl (2014); Erhard and Strauch (2013b), and Fagiano et al. (2014a) mention the limited

⋆ This research was supported by the Swiss National Science Foundation (Synergia) No. 141836 and the Swiss Commission for Technology and Innovation (CTI).
[1] Corresponding author

applicability of GPS measurements due to the slow update frequency. Millane et al. (2015) fuse readings from an IMU and measurements from Ultra-Wideband (UWB) range beacons, scattered on the ground and attached to a wing in a multiplicative error-state extended Kalman filter (EKF).

The use of onboard measurements is hindered by telemetry failures and time-varying delays due to fast system dynamics. Position measurements, extracted from a video footage of a camera mounted on the tether lead-out at the GS, have revealed that line angle measurements are affected by a time-varying delay up to two seconds and tether sag, Hesse et al. (2016). Consequently, an EKF with an augmented state vector to actively account for dead-times in an AWE system is proposed by Hesse et al. (2016). Measurements from an IMU are used to propagate the augmented error-state vector in an EKF, and line angle measurements are fused, assuming a constant delay.

State estimation for small Unmanned Aerial Vehicles (UAVs) involves dynamically delayed measurements, e.g camera measurements which are not necessarily temporally aligned with measurements from an IMU. Estimators for the pose of a UAV, which incorporate delay estimation, have been presented in Kelly (2011) and Li and Mourikis (2014). Both are based on a multiplicative error-state EKF and require reliable three-dimensional measurements from gyroscopes, magnetometers, accelerometers, and a position sensor. In the first work, estimation of a constant temporal shift is realised via an iterative closest point estimation in a preliminary calibration procedure. The second one incorporates a dynamic time-varying delay state in its process model.

In this work, we present a novel kinematic model to describe the motion of a tethered rigid wing. The wing and the tethers are modeled as a coupled system. The model is applied in a unscented Kalman filter (UKF) to fuse measurements of a gyroscope, line angle sensors and a camera. The state of the wing and model parameters, such as a dynamic tether delay, are estimated simultaneously. The estimator is compared to a state-of-the-art estimator, Hesse et al. (2016), using experimental flight data.

2. SYSTEM DESCRIPTION

The motion of the wing is defined in terms of the two right-handed reference frames defined in Figure 1. We follow the definitions in Hesse et al. (2016). The quarter-sphere, $\{(x, y, z) \in \mathbf{R}^3 | x > 0, z > 0, x^2 + y^2 + z^2 \leq r^2\}$, with radius, r, and its center at the origin of inertial frame, $\{G\}$, is referred to as the wind-window.

For a distance, $r(t)$, the wing position, $p(t)$, is expressed in the inertial frame, $\{G\}$, using spherical coordinates $\phi(t)$ and $\theta(t)$ as

$$p(t) = [\phi(t) \quad \theta(t) \quad r(t)]^T, \tag{1}$$

where the azimuth angle, $\phi(t) \in [-\pi, \pi]$, is the angle between the e_{Gx}-axis and the projection of $p(t)$ on the (e_{Gx}, e_{Gy})-plane, and the elevation angle, $\theta(t) \in [0, \pi]$, is the angle from the (e_{Gx}, e_{Gy})-plane towards the wing, Fagiano et al. (2014a).

The velocity vector of the wing, $v_L(t)$, expressed in the local frame, $\{L\}$, is given by

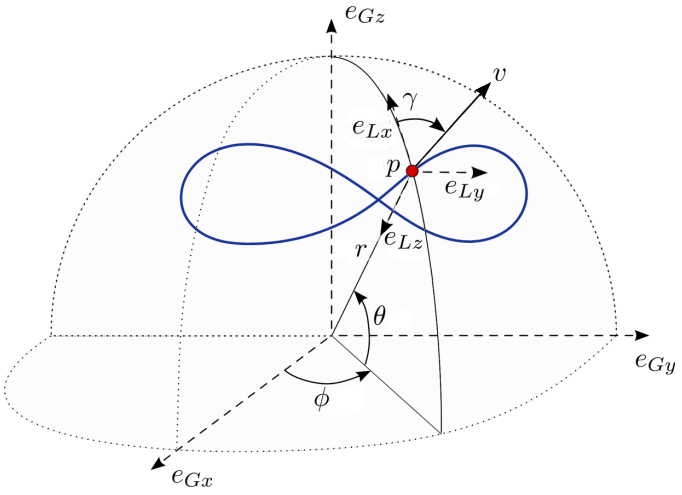

Fig. 1. The motion of the wing defined in terms of two reference frames, inertial frame $\{G\}$=(e_{Gx}, e_{Gy}, e_{Gz}) and local frame $\{L\}$=(e_{Lx}, e_{Ly}, e_{Lz}). The position, p, is defined by spherical angles, ϕ, θ, and distance, r. The magnitude of the tangential velocity is denoted by v, and the heading angle is given by γ.

$$v_L(t) = \begin{bmatrix} v_{Lx}(t) \\ v_{Ly}(t) \\ v_{Lz}(t) \end{bmatrix} = \begin{bmatrix} r(t)\dot{\theta}(t) \\ r(t)\cos(\theta(t))\dot{\phi}(t) \\ -\dot{r}(t) \end{bmatrix}. \tag{2}$$

The magnitude of the tangential velocity of the wing in the (e_{Lx}, e_{Ly})-plane, $v(t)$, can be written as,

$$\begin{aligned} v(t) &= \sqrt{v_{Lx}(t)^2 + v_{Ly}(t)^2} \\ &= r(t)\sqrt{\left(\cos(\theta(t))\dot{\phi}(t)\right)^2 + \left(\dot{\theta}(t)\right)^2}. \end{aligned} \tag{3}$$

The notion of the tangential velocity vector orientation has been demonstrated as a crucial feedback variable for the control of kites, Erhard and Strauch (2013a); Fagiano et al. (2014b); Zgraggen (2014). The tangential velocity vector orientation is

$$\begin{aligned} \gamma(t) &= \arctan_2\left(v_{Lx}(t), v_{Ly}(t)\right) \\ &= \arctan_2\left(\cos\left(\theta(t)\right)\dot{\phi}(t), \dot{\theta}(t)\right), \end{aligned} \tag{4}$$

where $\arctan_2(\cdot,\cdot) \in [-\pi, \pi]$ is the 4-quadrant arc tangent function. More details on the derivation of the tangential velocity vector orientation, which can also be interpreted as heading angle, can be found in Fagiano et al. (2014b).

Line angle sensors mounted on the lead-outs at the GS measure the wing position, $(\tilde{\phi}'(t), \tilde{\theta}'(t))$. A line length sensor measures the distance, $r(t)$, from the GS to the wing. A camera at the GS tracks the wing position, $(\tilde{\phi}(t), \tilde{\theta}(t))$, in a video stream. Finally, a gyroscope mounted on the wing measures the yaw rate, $\tilde{\omega}(t)$, which is transmitted to the GS using telemetry. Line angle measurements at the GS are sampled at 100 Hz. They are always available but known to be biased, Hesse et al. (2016). Visually tracked positions are extracted in 30 images per second. They are not available during intermittent target losses. Gyroscope measurements are transmitted at 30 Hz but may temporally not be available during telemetry failures.

3. MODELLING FOR STATE ESTIMATION

We introduce a novel kinematic model to describe the motion of a tethered soft or rigid wing. The model is motivated by system identification experiments using recorded log data from the kite power system described in Luchsinger et al. (2016). We first recall the unicycle model which is subsequently extended to a dual unicycle model to incorporate tether dynamics.

3.1 Unicycle Model

In traction phases, when the wing flies in crosswind conditions, we assume its trajectory lies on the surface of a sphere. For wings without depowering capabilities this assumption also holds in retraction phases. A unicycle model has been applied to model the motion of a wing on the surface of a sphere by Erhard and Strauch (2013a) and Wood et al. (2015b). The corresponding kinematic equations are

$$\dot{\phi}(t) = \frac{v(t)}{r(t)\cos\left(\theta(t)\right)}\sin\left(\gamma(t)\right), \tag{5a}$$

$$\dot{\theta}(t) = \frac{v(t)}{r(t)}\cos\left(\gamma(t)\right), \tag{5b}$$

$$\dot{\gamma}(t) = \frac{v(t)}{r(t)}\tan\left(\theta(t)\right)\sin\left(\gamma(t)\right) + \omega(t), \tag{5c}$$

where the turn-rate, $\omega(t)$, the velocity in the direction of motion, $v(t)$, and the distance, $r(t)$, are inputs. (5a) and (5b) express the dynamics of the position in spherical coordinates, $\phi(t)$, and $\theta(t)$. (5c) models the change of the heading angle, $\gamma(t)$. The trajectory lies on the sphere with radius, $r(t)$, and is shaped by the inputs, $v(t)$, and $\omega(t)$.

3.2 Dual Unicycle Model

In existing estimators for AWE, which fuse sensor measurements based on a unicycle model, the tethers are assumed to be rigid, Erhard and Strauch (2013a). Thus, measurements from line angle sensors at the GS are assumed to point towards the wing. Test flights have shown that this assumption is often violated and tether dynamics are not negligible, Hesse et al. (2016). As seen from the perspective of the wing, line angles measured at the ground follow the wing with a temporal delay, $t_d(t)$, and move slower by a velocity difference, $v_d(t)$.

We extend the unicycle model by projecting ground-based line angles to the sphere with radius, $r(t)$, with the kinematics of a second unicycle,

$$\dot{\phi}'(t) = \frac{v'(t)}{r(t)\cos\left(\theta'(t)\right)}\sin\left(\gamma'(t)\right), \tag{6a}$$

$$\dot{\theta}'(t) = \frac{v'(t)}{r(t)}\cos\left(\gamma'(t)\right), \tag{6b}$$

where the inputs, $\gamma'(t)$ and $v'(t)$ are coupled to the state of the wing. We denote variables related to the second unicycle, which represent the tethers following the wing, with a prime index. The velocity of the second unicycle, $v'(t)$, is modeled as differing from the velocity of the wing, $v(t)$, by a constant offset, v_d,

$$v'(t) = v(t) - v_d. \tag{7a}$$

The heading angle of the second unicycle, $\gamma'(t)$, is a delayed and scaled version of the wing heading angle, $\gamma(t)$,

$$\gamma'(t) = \lambda\gamma(t - t_d), \tag{7b}$$

Table 1. Three novel estimators fuse measurements from a camera ($\tilde{\text{C}}$), a gyroscope (Gyro), and line angle sensors ($\tilde{\text{LA}}$). They are compared to a state-of-the-art estimator (LA/Uni), Hesse et al. (2016).

Name	Process model	Sensors
LA/Uni	Unicycle	$\tilde{\text{LA}}$+Gyro
C/Uni	Unicycle	$\tilde{\text{C}}$+Gyro
LA/C/Uni	Unicycle	$\tilde{\text{LA}}$ + $\tilde{\text{C}}$+Gyro
LA/C/2Uni	Dual-Unicycle	$\tilde{\text{LA}}$ + $\tilde{\text{C}}$+Gyro

where the heading angle delay, t_d, and the scaling parameter, λ, are modeled as constants. The coupled model is motivated by leader follower dynamics of unicycles moving on a plane, Marshall (2005). The additional scaling parameter, λ, is required to ensure closed loops of the second unicycle when following a wing which flies figures-of-eight (typically, $\lambda \approx 1$). In the remainder of this work, we refer to the model described by (5) as the unicycle model and to the model described through the kinematics given by (5), (6) with the coupling from (7) as the dual unicycle model.

4. STATE AND PARAMETER ESTIMATION WITH DELAYED MEASUREMENTS

We introduce a novel state estimator which fuses sensor measurements in a UKF using the dual unicycle model from the Section 3.2. Further, we present two simplified estimators based on a unicycle model. The estimators apply two different measurement models and will be compared in Section 5. A summary is given in Table 1.

The UKF is an extension of the linear Kalman filter to nonlinear process and measurement models. Similar to the EKF it is a recursive filter that estimates the state of a dynamic system in a prediction step using a nonlinear process model and corrects the predicted state when new measurements become available. Contrary to the EKF, which is based on a first-order linearization, the UKF applies the unscented Transform to approximate the probability distributions of the optimal recursive Bayesian filter. A detailed review of the UKF is beyond the scope of this work. For more information, we refer the interested reader to van der Merwe et al. (2004).

The two unicycle-based estimators apply the unicycle model from Section 3.1 to predict the wing state when no measurements are available. The discrete kinematic model using forward-Euler integration reads as,

$$\phi(k+1) = \phi(k) + T_s\frac{v(k)}{r(k)\cos(\theta(k))}\sin\left(\gamma(k)\right) + q_\phi, \tag{8a}$$

$$\theta(k+1) = \theta(k) + T_s\frac{v(k)}{r(k)}\cos\left(\gamma(k)\right) + q_\theta, \tag{8b}$$

$$\gamma(k+1) = \gamma(k) + T_s\frac{v(k)}{r(k)}\tan(\theta(k))\sin(\gamma(k)) + T_s\omega(k) + q_\gamma, \tag{8c}$$

where q_ϕ, q_θ, q_γ are random variables modelling process noise. The state is augmented with noise-driven states

$$\omega(k+1) = \omega(k) + q_\omega, \tag{8d}$$

$$v(k+1) = v(k) + q_v, \tag{8e}$$

$$r(k+1) = r(k) + q_r, \tag{8f}$$

with q_ω, q_v, q_r being random variables. We model the process noise terms, q_ϕ, q_θ, q_γ, q_ω, q_v, q_r, as independent

white Gaussian noise with variances, $\sigma_\phi^2{=}10^{-4}$, $\sigma_\theta^2{=}10^{-4}$, $\sigma_\gamma^2{=}10^{-2}$, $\sigma_\omega^2{=}10^{-2}$, $\sigma_v^2{=}10^{-1}$, $\sigma_r^2{=}10^{-3}$, to capture errors from discretization and model mismatch.

The two unicycle estimators differ in the measurements used during the update step. The first one (C/Uni) fuses visually tracked positions with gyroscope measurements of an IMU. The linear measurement model is,

$$\tilde{\phi}(k) = \phi(k) + r_\phi, \tag{9a}$$
$$\tilde{\theta}(k) = \theta(k) + r_\theta, \tag{9b}$$
$$\tilde{\omega}(k) = \omega(k) + r_\omega, \tag{9c}$$

where we model measurement noise, $r_\phi, r_\theta, r_\omega$, as independent additive white Gaussian noise with variances $\kappa_\phi^2{=}10^{-3}$, $\kappa_\theta^2{=}10^{-3}$, $\kappa_\omega^2{=}10^{-1}$. The second one (LA/C/Uni) additionally fuses line angle measurements,

$$\tilde{\phi}(k) = \phi'(k) + r_{\phi'}, \tag{10a}$$
$$\tilde{\theta}(k) = \theta'(k) + r_{\theta'}, \tag{10b}$$

where the measurement noise terms $r_{\phi'}$, and $r_{\theta'}$, are modeled as independent white Gaussian noise with variances $\kappa_{\phi'}^2{=}10^{-3}$, $\kappa_{\theta'}^2{=}10^{-3}$. Note, for this estimator measurements from line angle sensors are assumed to be unbiased and to measure the true wing position, $\phi(t), \theta(t)$.

The third estimator (LA/C/2Uni) applies the dual unicycle model. The kinematic equations of motion for the wing are given by (8) and combined with the kinematics of a second unicycle as defined in Section 3.2,

$$\phi'(k+1) = \phi'(k) + T_s \frac{v'(k)}{r(k)\cos(\theta'(k))} \sin(\gamma'(k)) + q_{\phi'}, \tag{11a}$$

$$\theta'(k+1) = \theta'(k) + T_s \frac{v'(k)}{r(k)} \cos(\gamma'(k)) + q_{\theta'}, \tag{11b}$$

where we used forward-Euler integration and process noise is modeled as random variables $q_{\phi'}$ and $q_{\theta'}$. The process model is completed by states for the coupling terms,

$$t_d(k+1) = t_d(k) + q_{t_d}, \tag{11c}$$
$$v_d(k+1) = v_d(k) + q_{v_d}, \tag{11d}$$

which we model as noise-driven states with random variables q_{t_d} and q_{v_d}. The process noise terms are assumed to be independent white Gaussian noise with variances $\sigma_{\phi'}^2{=}10^{-4}$, $\sigma_{\theta'}^2{=}10^{-4}$, $\sigma_{t_d}^2{=}10^{-3}$, $\sigma_{v_d}^2{=}10^{-4}$. Hence, noise-driven states vary slowly over time in order to adapt to changing flight conditions. We want to point out, the variable delay is estimated as constraint state with $\hat{t}_d \in [0, t_{\max}]$. The scaling parameter is constant, $(\lambda = 1)$.

The dual unicycle estimator (LA/C/2Uni) uses line angle measurements, visually tracked positions and the measured turn-rate of the wing, to update a predicted state. The measurement equations are given by (9) and completed by line angle measurements

$$\tilde{\phi}'(k) = \phi'(k) + r_{\phi'}, \tag{12a}$$
$$\tilde{\theta}'(k) = \theta'(k) + r_{\theta'}, \tag{12b}$$

with $r_{\phi'}$ and $r_{\theta'}$ being the same random variables as in (10). Note that, the line angle measurements are used to correct the position of the second unicycle rather than the position of the wing as in unicycle-based estimators.

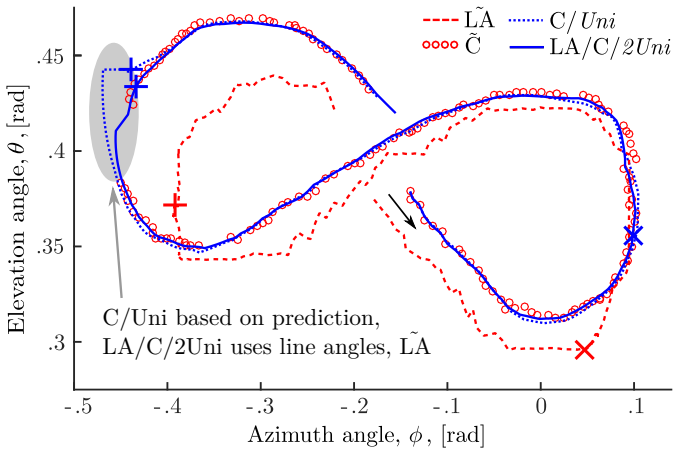

(a) The estimated wing trajectories in the ϕ-θ-plane and camera (red circles) and line angle (dashed red) measurements.

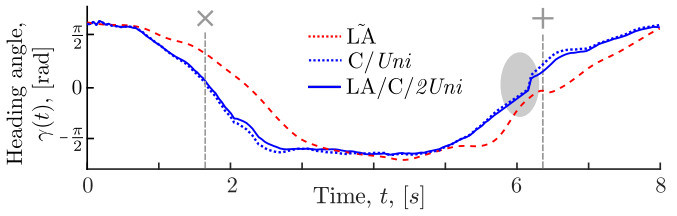

(b) The heading angle estimates, $\hat{\gamma}$, corresponding to the estimated trajectory in (a). The dashed red line indicates the estimated heading angle, $\hat{\gamma}$, based on line angles only.

Fig. 2. Estimation results for the most important feedback variables are shown. Estimates of the dual unicycle estimator (LA/C/2Uni) are shown as solid blue line; those of the unicycle estimator (C/Uni) as a dashed blue line. The markers, × and +, indicate two simultaneous time steps on the trajectories. The grey areas highlight where camera measurements are missing.

5. EXPERIMENTAL RESULTS

We demonstrate the applicability of the kinematic models and estimators using experimental data gathered with the AWE system described in Luchsinger et al. (2016). We investigate the estimation performance on important feedback variables, i.e. position, (ϕ, θ), heading angle, γ, and model parameters such as line angle delay, t_d, and velocity difference, v_d. We compare estimation results to the state-of-the-art estimator (LA/Uni) based on line angle and gyroscope measurements from Hesse et al. (2016). The experimental data is recorded during three test flights with different wings and wind conditions. It covers more than 120 minutes of flight time and includes tractions and retractions. When camera measurements are missing, e.g. the wing flies in a cloud, we assume gyroscope measurements to be missing as well in order to increase the complexity of the estimation problem. In this case, the estimators predict the state based on the process models, where those which fuse line angle sensing update the state using measured line angles only. The initial covariance of all estimators is selected to be an identity matrix.

Figure 2a shows line angle and camera measurements as well as the estimated positions, $\hat{\phi}$, $\hat{\theta}$ of the estimators (C/Uni, LA/C/2Uni) for a representative figure-of-eight path. Figure 2b shows the corresponding estimated head-

ing angle, $\hat{\gamma}$. Further estimators (LA/Uni, LA/C/Uni) are not shown because of significant quality degradation due to biased line angle measurements. Both estimators (C/Uni, LA/C/2Uni) track the position and heading angle well, when all measurements are available. The dual unicycle estimator (LA/C/2Uni) has improved prediction capabilities compared to the unicycle estimator (C/Uni) when camera measurements are missing. We observe a smaller drift of the dual unicycle estimator when observations are missing due to the additionally fused line angle measurements and the estimated coupling parameters, v_d and t_d.

Figure 3 shows estimation results of the dual unicycle estimator (LA/C/2Uni) for the state of the wing and model parameters, e.g. the delay, $\hat{t}_d$, and velocity difference, $\hat{v}_d$, over an interval of 100 seconds with nine figure-of-eights. We obtain the true heading angle delay, t_d, using the least-square method from Wood et al. (2015a). The estimated heading angle delay, $\hat{t}_d$, is close to the true heading angle, t_d. We observe that the heading angle delay, t_d, increases with longer tethers, r. The estimated heading angle delay, $\hat{t}_d$, varies more than the true heading angle delay, t_d, since it is estimated as a noise-driven state, see Figure 3.

In order to compare the estimation performance of all estimators in Table 1, we define the average errors for the estimated wing positions of the wing, $\hat{\phi}$, $\hat{\theta}$, as

$$\bar{\epsilon} = E\left\{\arccos\left(\cos\left(\phi-\hat{\phi}\right)\cos\left(\theta-\hat{\theta}\right)\right)\right\} \tag{13}$$

applying the spherical equivalent of the Pythagorean theorem, and for the estimated heading angles as

$$\bar{\gamma}_{err} = E\left\{|\gamma-\hat{\gamma}|\right\}. \tag{14}$$

The average errors, $\bar{\epsilon}$, over 120 flight minutes are shown in Figure 4a for the estimated wing position and in Figure 4b for the estimated heading angle, respectively. In addition to the estimators presented here, we show estimation results for the state-of-the-art estimator from Hesse et al. (2016) which fuses line angle measurements with turn-rate measurements of a gyroscope but does not incorporate visually tracked positions (LA/Uni).

Estimators which fuse camera measurements (C/Uni, LA/C/Uni, LA/C/2Uni) return superior position estimates compared to a line angle based approach (LA/Uni), even though measurements are occasionally missing, see Figure 2. The unicycle-based estimator, which fuses camera and line angle measurements (LA/C/Uni), shows degraded performance since line angles are erroneously assumed to be unbiased. Gyroscope measurements can compensate for errors in biased line angle measurements when the heading angle is estimated. In the experimental flights considered here, the camera tracks the wing reliably for the most part and interruptions are limited to brief periods. In addition to the position and heading angle, the approach presented here incorporates the estimation of model parameters. In particular, the estimated delay can be used for the development of an improved controller, Wood et al. (2015a).

6. CONCLUSIONS

The achievable cycle efficiency of airborne wind energy systems is limited by estimation delay. Unobservable tether dynamics in ground-based systems which rely solely on

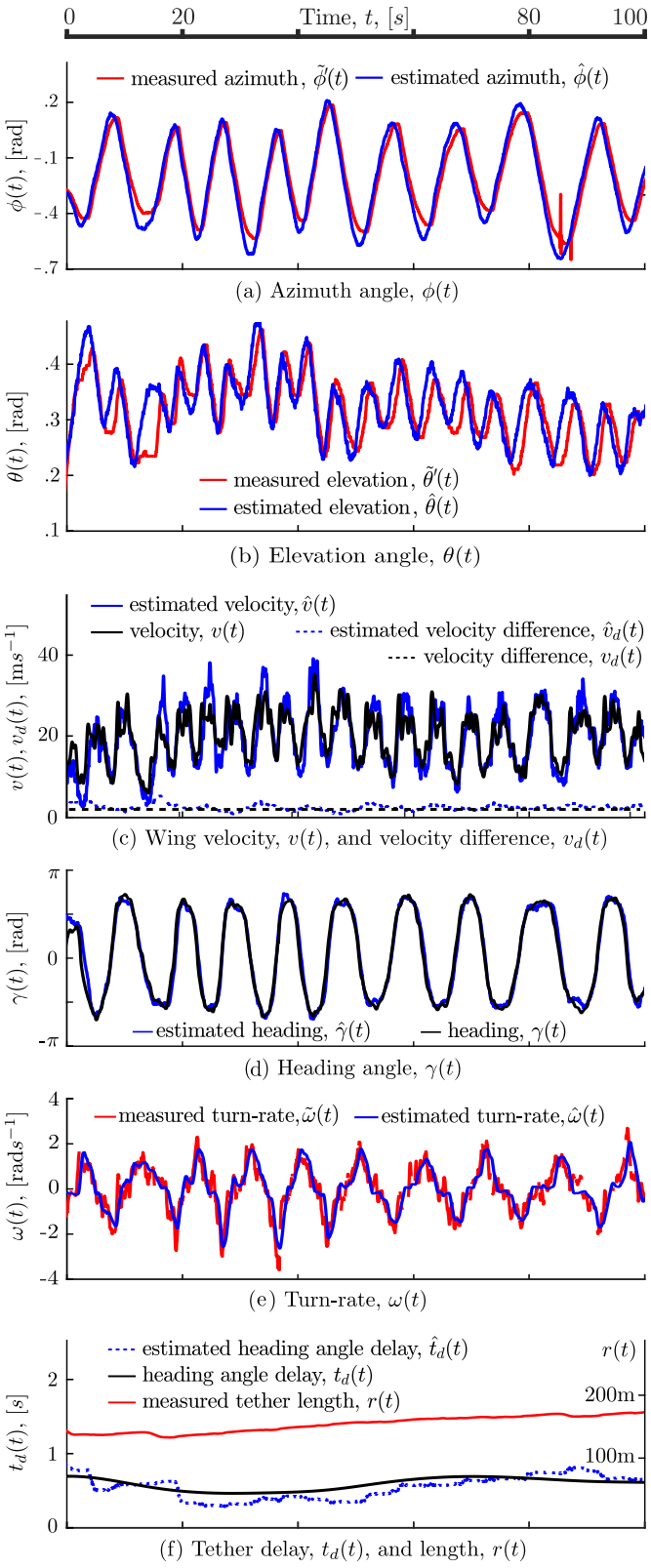

Fig. 3. Estimation results for a tethered rigid wing, which flies nine representative figure-of-eights, using a UKF and a dual unicycle model (LA/C/2Uni). Line angle, tether length and gyroscope measurements are shown as red lines. The estimated wing state and model parameters are shown as solid and dashed blue lines, respectively. Reference values extracted in a post-processing step are shown as black lines.

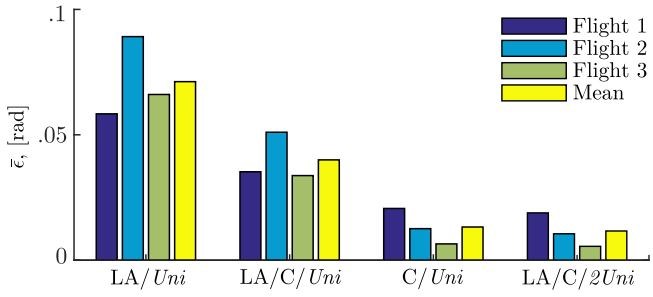

(a) Mean error of the estimated position, $\bar{\epsilon}$.

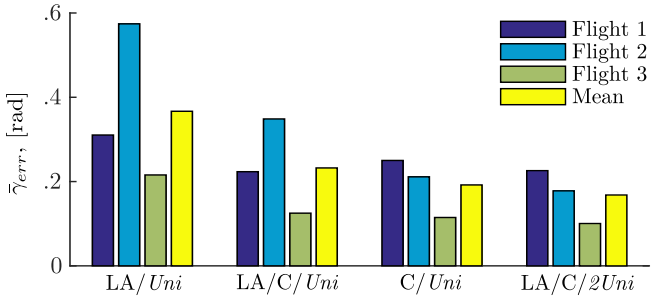

(b) Mean error of the estimated heading angle, $\bar{\gamma}$.

Fig. 4. Errors of four estimators in three flights are shown for the position, $\bar{\epsilon}$, in (a) and the heading angle, $\bar{\gamma}_{err}$, in (b). The errors are defined as deviation from the true trajectory as obtained in a post-processing step.

line sensing aggravates the situation. This work focuses on new estimation schemes that fuse additional sensor measurements. Based on a novel dual unicycle model of tethered wing kinematics, we have applied an unscented Kalman filter to fuse visually tracked position measurements with measurements from inertial sensors and line sensors. The effect of tether dynamics, such as tether sag and induced dead-time, is addressed by incorporating the estimation of model parameters directly in the estimation process. We have demonstrated the applicability of the estimator using experimental data. The estimation scheme can be extended to fuse further measurements, such as those obtained from UWB range beacons or GPS sensors.

ACKNOWLEDGEMENTS

We acknowledge Corey Houle, Damian Aregger, Janis Heilmann from FHNW and Dino Costa, Cédric Galliot and Florian Bezard from Empa for support with the experimental tests. The advice of Flavio Gohl and Rolf Luchsinger from TwingTec is also gratefully acknowledged.

REFERENCES

Cherubini, A., Papini, A., Vertechy, R., and Fontana, M. (2015). Airborne Wind Energy Systems: A Review of the Technologies. *Renewable and Sustainable Energy Reviews*, 51, 1461–1476.

Erhard, M. and Strauch, H. (2013a). Control of Towing Kites for Seagoing Vessels. *IEEE Transactions on Control Systems Technology*, 21(5), 1629–1640.

Erhard, M. and Strauch, H. (2013b). Sensors and Navigation Algorithms for Flight Control of Tethered Kites. In *European Control Conf. (ECC)*, 998–1003.

Fagiano, L., Huynh, K., Bamieh, B., and Khammash, M. (2014a). On Sensor Fusion for Airborne Wind Energy Systems. *IEEE Transactions on Control Systems Technology*, 22(3), 930–943.

Fagiano, L., Zgraggen, A.U., Morari, M., and Khammash, M. (2014b). Automatic Crosswind Flight of Tethered Wings for Airborne Wind Energy: Modeling, Control Design, and Experimental Results. *IEEE Transactions on Control Systems Technology*, 22(4), 1433–1447.

Goela, J.S. (1979). Wind Power Through Kites. *Mechanical Engineering*, 101(6), 42–43.

Gros, S., Zanon, M., and Diehl, M. (2012). Orbit Control for a Power Generating Airfoil Based on Non-Linear MPC. In *American Control Conf. (ACC)*, 137–142.

Hesse, H., Polzin, M., Wood, T.A., and Smith, R.S. (2016). Visual Motion Tracking and Sensor Fusion for Ground-Based Kite Power Systems. In *Airborne Wind Energy*. Springer, Berlin, [in press].

Jehle, C. and Schmehl, R. (2014). Applied Tracking Control for Kite Power Systems. *Journal of Guidance, Control, and Dynamics*, 37(4), 1211–1222.

Kelly, J.S. (2011). *On Temporal and Spatial Calibration for High Accuracy Visual-Inertial Motion Estimation*. Ph.D. thesis, University of Southern California.

Li, M. and Mourikis, A.I. (2014). Online Temporal Calibration for Camera-IMU Systems: Theory and Algorithms. *International Journal of Robotics Research*, 33(7), 947–964.

Luchsinger, R.H., Aregger, D., Bezard, F., Costa, D., Galliot, C., Gohl, F., Heilmann, J., Hesse, H., Houle, C., Wood, T.A., and Smith, R.S. (2016). Pumping Cycle Kite Power with Twings. In *Airborne Wind Energy*. Springer, Berlin, [in press].

Marshall, J. (2005). *Coordinated Autonomy: Pursuit Formations of Multivehicle Systems*. Ph.D. thesis, University of Toronto.

Millane, A., Hesse, H., Wood, T.A., and Smith, R.S. (2015). Range-Inertial Estimation for Airborne Wind Energy. *Conf. on Decision & Control*, 455–460.

van der Merwe, R., Wan, E., and Julier, S. (2004). Sigma-Point Kalman Filters for Nonlinear Estimation and Sensor-Fusion: Applications to Integrated Navigation. In *Guidance, Navigation, and Control Conf.*, 16–19.

Wood, T.A., Hesse, H., Zgraggen, A.U., and Smith, R.S. (2015a). Model-Based Flight Path Planning and Tracking for Tethered Wings. *Conf. on Decision & Control*, 6712–6717.

Wood, T.A., Hesse, H., Zgraggen, A.U., and Smith, R.S. (2015b). Model-Based Identification and Control of the Velocity Vector Orientation for Autonomous Kites. In *American Control Conf.*, 2377–2382.

Zgraggen, A.U., Fagiano, L., and Morari, M. (2015). Real-Time Optimization and Adaptation of the Crosswind Flight of Tethered Wings for Airborne Wind Energy. *IEEE Transactions on Control Systems Technology*, 23(2), 434–448.

Zgraggen, A.U. (2014). *Automatic Power Cycles for Airborne Wind Energy Generators*. Ph.D. thesis, ETH Zürich.